Ninth International Conference on Computational Fluid Dynamics (ICCFD9), Istanbul, Turkey, July 11-15, 2016

ICCFD9-xxxx

A Front-Tracking Method for Direct Numerical Simulation of Viscoelastic Interfacial Flows

Daulet Izbassarov & Metin Muradoglu

Department of Mechanical Engineering, Koc University, Istanbul 34450, Turkey
Corresponding author: dizbassarov@ku.edu.tr

Abstract: We present a front-tracking method developed for direct numerical simulations of viscoelastic two-phase systems in which one or both phases could be viscoelastic. The method is designed to incorporate virtually any viscoelastic fluid model belonging to the family of the Oldroyd-B and FENE. The viscoelastic model equations are solved fully coupled with the flow equations within the front-tracking framework. The convective terms of the viscoelastic model equations are approximated using a fifth order WENO-Z scheme that is found to be instrumental for resolving the viscoelastic stress boundary layer near the interface. A log-conformation method is employed to overcome the high Weissenberg number problem (HWNP) and found to be stable and very robust for a wide range of Weissenberg numbers. The method has been first validated for various benchmark single-phase and two-phase viscoelastic flow problems. Then it has been applied to study effects of viscoelasticity on drop dynamics in a capillary tube as well as on drop impact and spreading on a solid wall.

Keywords: Front-Tracking Method, Viscoelasticity, Multiphase Flows, Microfluidics, Moving Contact Line.

1 Introduction

Understanding and modeling of viscoelastic flows is of fundamental importance in a wide range of engineering applications such as materials and food processing, pharmaceuticals, polymer blends and droplet-based micro/bio-fluidics [1]. Mathematical models are usually based on the dumbbell assumption and results in highly non-linear system of differential equations. Numerous studies of viscoelastic flows using one or more non-linear differential models with different discretization techniques including finite element, finite difference and finite volume methods can be found in the literature [2]. It has been long recognized that modeling of viscoelastic interfacial flows is a challenging task mainly due to the existence of moving and deforming interface separating phases and large disparity in time scales especially at high Weissenberg numbers. The front-tracking method has been proven to be a viable tool for simulation of interfacial flows with multi-physics effects and successfully applied to a wide range of multiphase flow problems [3, 4, 5, 6, 7].

In the present study, a finite difference-front tracking method is developed for direct numerical simulation of viscoelastic interfacial flows. Although the method is general and applicable to virtually any interfacial flows involving viscoelastic fluids, our main goal is to understand the drop dynamics encountered or inspired by micro/bio-fluidic applications. The method is designed to accommodate the generic family of viscoelastic model equations including the Oldroyd-B, FENE-CR of Chilcott Rallison [8] and FENE-MCR of Coates et al. [9]. The convective terms in viscoelastic constitutive equations are approximated using a fifth-order upwinded WENO-Z [10] schemes. All the other spatial derivatives are approximated using central differences on a staggered grid. The log-conformation method (LCM) is employed to overcome high Weissenberg number problem. The method has been first validated for a benchmark single-phase problem of the start-up Poiseuille flow in a circular capillary tube. Then the method is applied to simulate the motion and deformation of a

buoyancy-driven droplet in viscoelastic two-phase systems moving through a capillary tube. The results for both single and two phase systems are found to be in good agreement with available analytical solution and numerical results. Finally the method has been successfully applied to a more challenging cases involving motion and deformation of a droplet in pressure-driven viscoelastic two-phase systems and viscoelastic drop impact and spreading on a flat solid surface. The present numerical algorithm has been found to be very robust and grid convergent with second-order spatial accuracy for all the cases considered in this paper.

2 Formulation and numerical method

The governing equations are described in the framework of the finite-difference/front-tracking method. The flow is assumed to be incompressible. Following Unverdi and Tryggvason [11] and Izbassarov and Muradoglu [5], a single set of conservation equations are solved for the entire domain including the dispersed and the continuous phases. The continuity and momentum equations can be written as follows:

$$\nabla \cdot \mathbf{u} = 0, \tag{1}$$

$$\frac{\partial \rho \mathbf{u}}{\partial t} + \nabla \cdot (\rho \mathbf{u}\mathbf{u}) = -\nabla p + \nabla \cdot \mu_s (\nabla \mathbf{u} + \nabla \mathbf{u}^T) + \nabla \cdot \boldsymbol{\tau} + \int_A \gamma \kappa \mathbf{n} \delta(\mathbf{x} - \mathbf{x_f}) dA, \tag{2}$$

where μ_s, ρ, p, $\mathbf{u}$ and $\boldsymbol{\tau}$ denote the solvent viscosity, the density, the pressure, the velocity vector and the viscoelastic extra stress tensor, respectively. The last term in Eq. (2) represents the body force due to surface tension where γ is the surface tension coefficient, κ is twice the mean curvature, and $\mathbf{n}$ is the unit vector normal to the interface. The surface tension acts only on the interface as indicated by the three-dimensional delta function, δ, whose arguments $\mathbf{x}$ and $\mathbf{x_f}$ are the points at which the equation is being evaluated and a point at the interface, respectively.

The Oldroyd-B, FENE-CR and FENE-MCR models are adopted as the constitutive equations for the viscoelastic extra stresses. These models can be written in a generic transport equation form as

$$\frac{\lambda}{F}\left(\frac{\partial \mathbf{E}}{\partial t} + \nabla \cdot (\mathbf{u}\mathbf{E}) - (\nabla \mathbf{u})^T \cdot \mathbf{E} - \mathbf{E} \cdot \nabla \mathbf{u}\right) + \mathbf{E} = \mathbf{S}, \tag{3}$$

where $\mathbf{E}$ can be extra stress or conformation tensor and $\mathbf{S}$ is a source term. In Eq. (3), F, $\mathbf{S}$ and $\boldsymbol{\tau}$ are specified in Table 1 for the three viscoelastic models considered in the present study. In this table, μ_p, λ, L, F, $\mathbf{I}$ and $\boldsymbol{\tau}$ are the polymeric viscosity, the relaxation time, the ratio of the length of a fully extended polymer dumbbell to its equilibrium length, the stretch function, the identity and extra stress tensors, respectively. The conformation tensor is then defined as

$$\mathbf{A} = \frac{\lambda}{\mu_p F}\boldsymbol{\tau} + \mathbf{I}. \tag{4}$$

Table 1: Specification of the parameters F, $\mathbf{S}$ and $\boldsymbol{\tau}$ in Eq. (3).

Model	F	$\mathbf{S}$	$\boldsymbol{\tau}$
Oldroyd-B	1	$\mathbf{I}$	$\mu_p F(\mathbf{E} - \mathbf{I})/\lambda$
FENE-CR	$L^2/(L^2 - \text{trace}(\mathbf{E}))$	$\mathbf{I}$	$\mu_p F(\mathbf{E} - \mathbf{I})/\lambda$
FENE-MCR	$(L^2 + \lambda \text{trace}(\mathbf{E})/\mu_p)/(L^2 - 3)$	$\mu_p(\nabla \mathbf{u} + \nabla \mathbf{u}^T)$	$\mathbf{E}$

Numerical solution of the viscoelastic constitutive equations is notoriously difficult especially in two-phase systems mainly due to the large disparity in time scales and discontinuous variation of viscoelastic properties across the interfaces. To overcome these difficulties, the log-conformation method (LCM) developed by Fattal and Kupferman [12] is employed. The LCM is used to overcome the well known high Weissenberg number problem (HWNP). In this approach, Eq. (3) is rewritten in terms of the logarithm of the conformation tensor through eigen-decomposition, i.e., $\boldsymbol{\Psi} = \log \mathbf{A}$. This representation ensures the positive definiteness of the conformation tensor. The core feature of the formulation is the decomposition of the gradient of divergence

free velocity field $\nabla \mathbf{u}^T$ into two anti-symmetric tensors denoted by $\mathbf{\Omega}$ (pure rotation) and $\mathbf{N}$, and a symmetric tensor denoted by $\mathbf{C}$ which commutes with the conformation tensor [12], i.e.,

$$\nabla \mathbf{u}^T = \mathbf{\Omega} + \mathbf{C} + \mathbf{N}\mathbf{A}^{-1}. \tag{5}$$

Inserting Eq. (5) into Eq. (3) and replacing the conformation tensor with the new variable $\mathbf{\Psi}$, the transformed constitutive equations can be written as

$$\frac{\partial \mathbf{\Psi}}{\partial t} + \nabla \cdot (\mathbf{u}\mathbf{\Psi}) - (\mathbf{\Omega}\mathbf{\Psi} - \mathbf{\Psi}\mathbf{\Omega}) - 2\mathbf{C} \quad = \quad \frac{F}{\lambda}(e^{-\mathbf{\Psi}} - \mathbf{I}). \tag{6}$$

This equation is integrated using an explicit Euler scheme, i.e.,

$$\mathbf{\Psi}^{n+1} = \mathbf{\Psi}^n + \Delta t \left(-\nabla \cdot (\mathbf{u}\mathbf{\Psi}) + (\mathbf{\Omega}\mathbf{\Psi} - \mathbf{\Psi}\mathbf{\Omega}) + 2\mathbf{C} + \frac{F}{\lambda}(e^{-\mathbf{\Psi}} - \mathbf{I}) \right)^n, \tag{7}$$

where the spatial derivatives are again approximated using central differences except for the convective terms for which a fifth-order upwinded WENO-Z [10] scheme is employed. The conformation tensor is then obtained using the inverse transformation as $\mathbf{A} = e^{\mathbf{\Psi}}$.

The flow equations are solved fully coupled with the viscoelastic model equations using the front-tracking method developed by Izbassarov and Muradoglu [5]. A complete description of the front tracking method can be found in Tryggvason et al. [3] and the treatment of the viscoelasticity can be found in Izbassarov and Muradoglu [5].

3 Results and Discussion

3.1 Validation

The method is first validated for viscoelastic single-phase flows. The test case concerns with the start-up Poiseuille flow of an Oldroyd-B fluid in a circular pipe. Waters and King [13] first studied this problem and provided analytical solutions both for the transient and steady-state cases. Thus it serves an ideal test case for validation of the present numerical method. Computations are performed for three different Weissenberg numbers, i.e., $Wi = 1, 10$ and 100. Figure 1a shows the velocity profiles at various dimensionless times for $Wi = 10$. The evolution of the centerline velocity is plotted in Fig. 1b for $Wi = 1, 10$ and 100. As can be seen in these figures, there is excellent agreement between the computational and analytical results indicating the accurate solution of the viscoelastic model equations.

The method is then validated for the buoyancy-driven viscoelastic droplet systems studied computationally by You et al. [14]. The FENE-CR model is employed in the present simulations to facilitate direct comparison with the results of You et al. [14]. Note that You et al. [14] defined a slightly different conformation tensor that is related to $\mathbf{A}$ as $\mathbf{B} = \mathbf{A} - \mathbf{I}$. The constant contours of the component B_{zz} of the conformation tensor are plotted in Fig. 2 in the vicinity of the droplet in a steady motion for a viscoelastic droplet in a Newtonian medium (VN) and a Newtonian droplet in a viscoelastic medium (NV), together with the computational results of You et al. [14]. These figures show that a Newtonian drop immersed in a viscoelastic fluid experiences an extending trailing edge while a viscoelastic drop in a Newtonian fluid develops an indentation around the rear stagnation point. Moreover, in both cases, there is a thin layer at the interface in the leading and trailing edges of the droplet where the viscoelastic stress concentration occurs with a sharp gradient due to large polymer extensions. These results are overall in good qualitative and quantitative agreement with the computational simulations of You et al. [14].

3.2 Pressure-driven viscoelastic two-phase systems in a capillary tube with sudden contraction and expansion

The method is then applied to study the viscoelastic two-phase systems in a capillary tube with a sudden contraction and expansion. Sample results are shown in Fig. 3 where the transient motion of a FENE-CR droplet moving through a Newtonian fluid is shown. As seen, just before entering the constriction, the

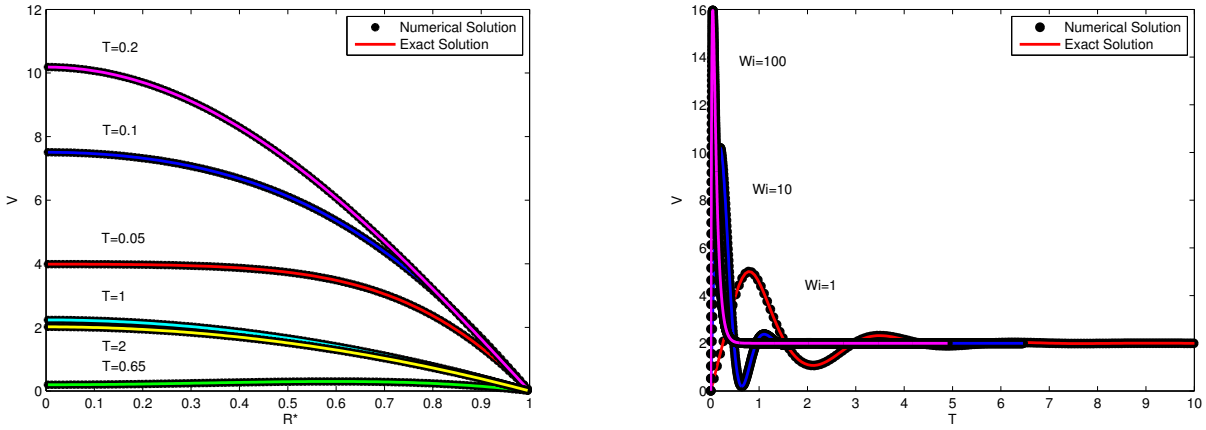

(a) (b)

Figure 1: The start-up Poiseuille flow: (a) The velocity profiles at different non-dimensional times for $Wi = 10$. (b) The evolution of centerline velocity for $Wi = 1, 10$ and 100. The symbols represent the computational results and the solid lines are the analytical solution of Waters and King [13].

viscoelastic stress concentration occurs at the shoulder of the droplet that acts against the viscous stresses to restore the indentation of the trailing edge. The re-entrant cavity grows continuously while the droplet is in the narrow channel and the entrained ambient fluid is eventually encapsulated within the main drop to form a bigger compound drop. It is evident that viscoelastic effects are important for the development of the re-entrant cavity. Therefore, further simulations are performed for various Wi numbers, and the results are shown in Fig. 4. It is interesting to observe that the viscoelasticity has a non-monotonic effect on the drop deformation, i.e., the size of the re-entrant cavity and resulting inner droplet first decrease and then increase with Wi.

3.3 Drop Impact and Spreading on a Solid Surface

Finally, we apply the method to study a viscoelastic drop impacting and spreading on a solid surface. Besides its practical importance, this problem is interesting since it involves a moving contact line making the problem a more difficult test case for the numerical method. Sample results are shown in Fig. 5 where the evolution of drop shapes are plotted for $Wi = 0$ (Newtonian), $Wi = 1$ and $Wi = 10$. As can be seen, the magnitude of the viscoelastic stresses monotonically increases as Wi is increased. However, unlike the Oldroyd-B model, the FENE-CR model bounds the growth of the viscoelastic stresses. Therefore the increase in the stresses gets smaller when Wi exceeds a threshold value, i.e., when $Wi \geq 10$ in this case. It is interesting to see that the viscoelasticity favors spreading of the droplet and the viscoelastic droplet tends to spread more than that of the Newtonian one, which is in agreement with the computational results of Tome et al. [15] and Fang et al. [16]. Whilst, there is no significant difference between $Wi = 1$ and $Wi = 10$ cases in the advancing phase. However, in the retraction phase, the difference gets more pronounced and the retraction becomes faster as Wi increases. When the retraction velocity is fast enough, the fluid rises up from the center of droplet forming a dome, which may even lead to a complete rebound from the substrate, see e.g., the $Wi = 10$ case in Fig. 5. A part of the initial kinetic energy is stored as the elastic energy in the viscoleastic drop during the advancing phase, which reduces the available energy for dissipation. This elastic energy is then released during the recoiling phase contributing to the drop rebound. This finding is in agreement with the experimental observation of Bertola [17]. An extensive study on the effects of viscoelasticity on drop impact and spreading on a solid surface can be found in Izbassarov and Muradoglu [7].

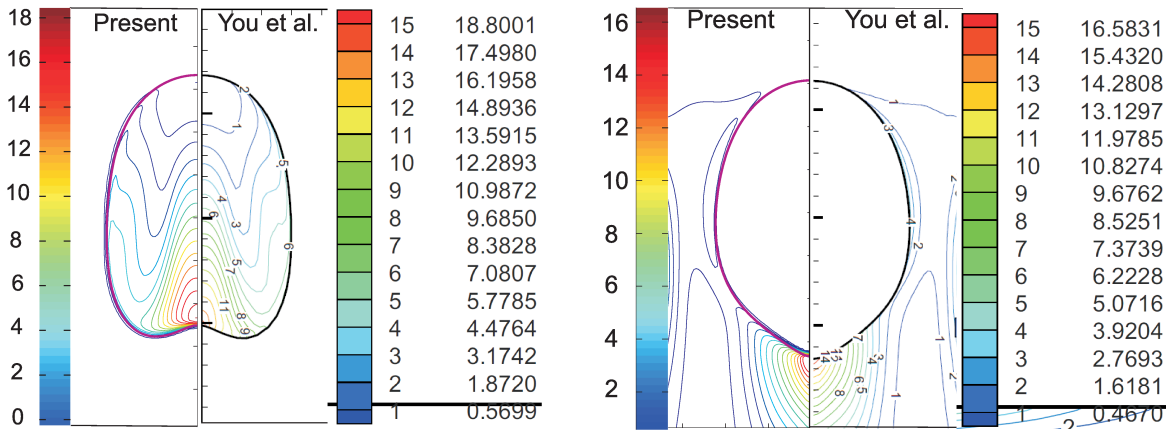

Figure 2: The steady droplet shapes and the constant contours of the conformation tensor component B_{zz} for a buoyancy-driven FENE-CR droplet rising in a Newtonian fluid (left) and Newtonian droplet rising in a FENE-CR fluid (right). The present results (left portion) are compared with the results of You et al. [14] (right portion). $(Re = 10, Ca = 50, Wi = 50, Grid : 128 \times 1184)$.

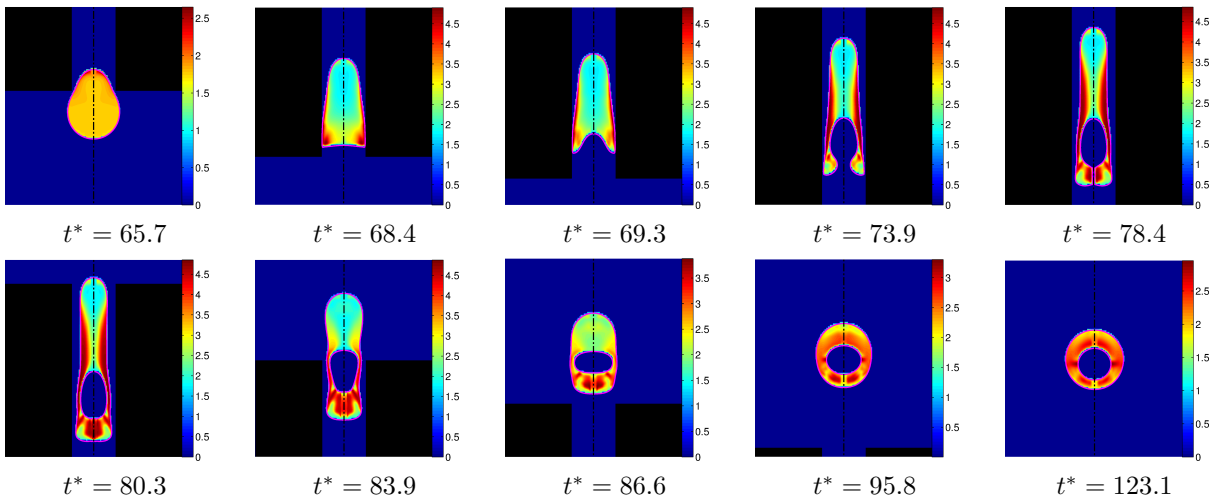

Figure 3: A FENE-CR droplet moving through a Newtonian fluid in a pressure driven contraction/expansion capillary tube. The contours represent the average polymer extension $\sqrt{\text{trace}(\mathbf{A})}$. $(Ca = 0.1, Re = 2, Wi = 100, \theta = 40, Grid : 64 \times 768)$.

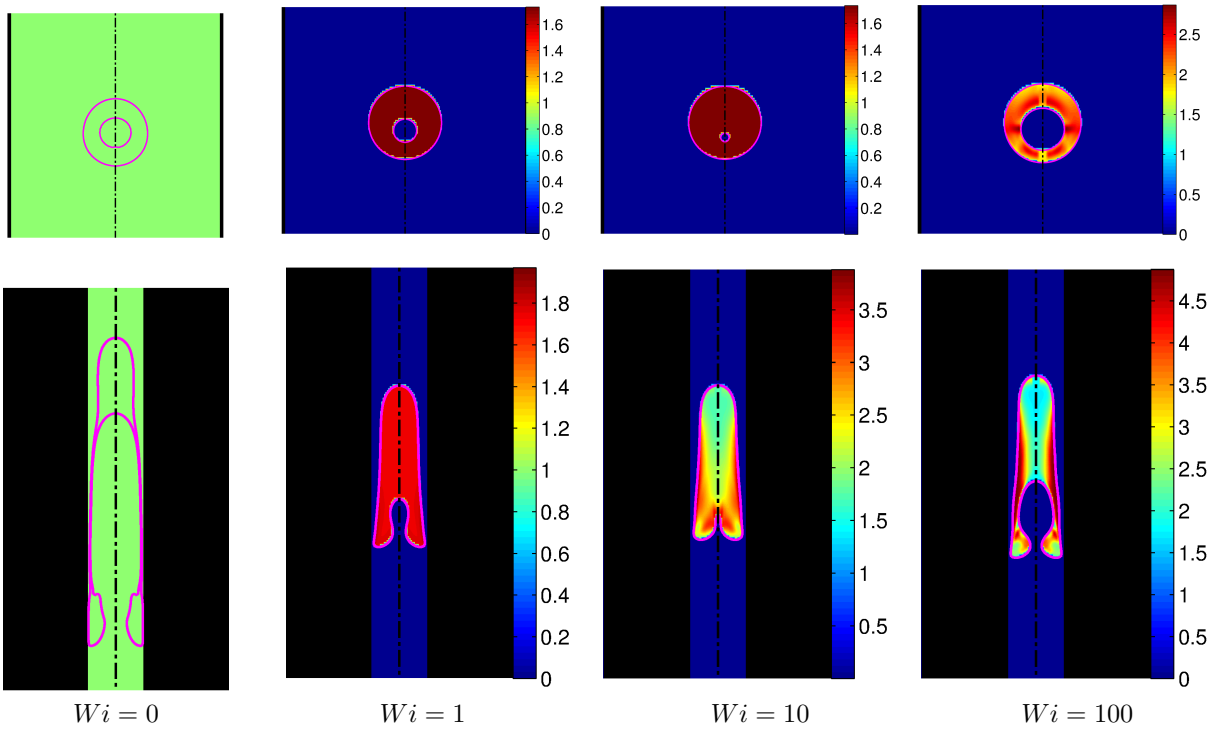

Figure 4: The effects of fluid elasticity on drop deformation at a high viscosity ratio of $\theta = 40$ for the NN and VN cases. The droplet shapes and the constant contours of the average polymer extension $\sqrt{\text{trace}(\mathbf{A})}$ are plotted in the vicinity of the droplet in the middle of the constriction (bottom plots) and in the further downstream of the expansion region (top plots). $(Ca = 0.1, Re = 2, \kappa = 1.25, Grid : 64 \times 768)$.

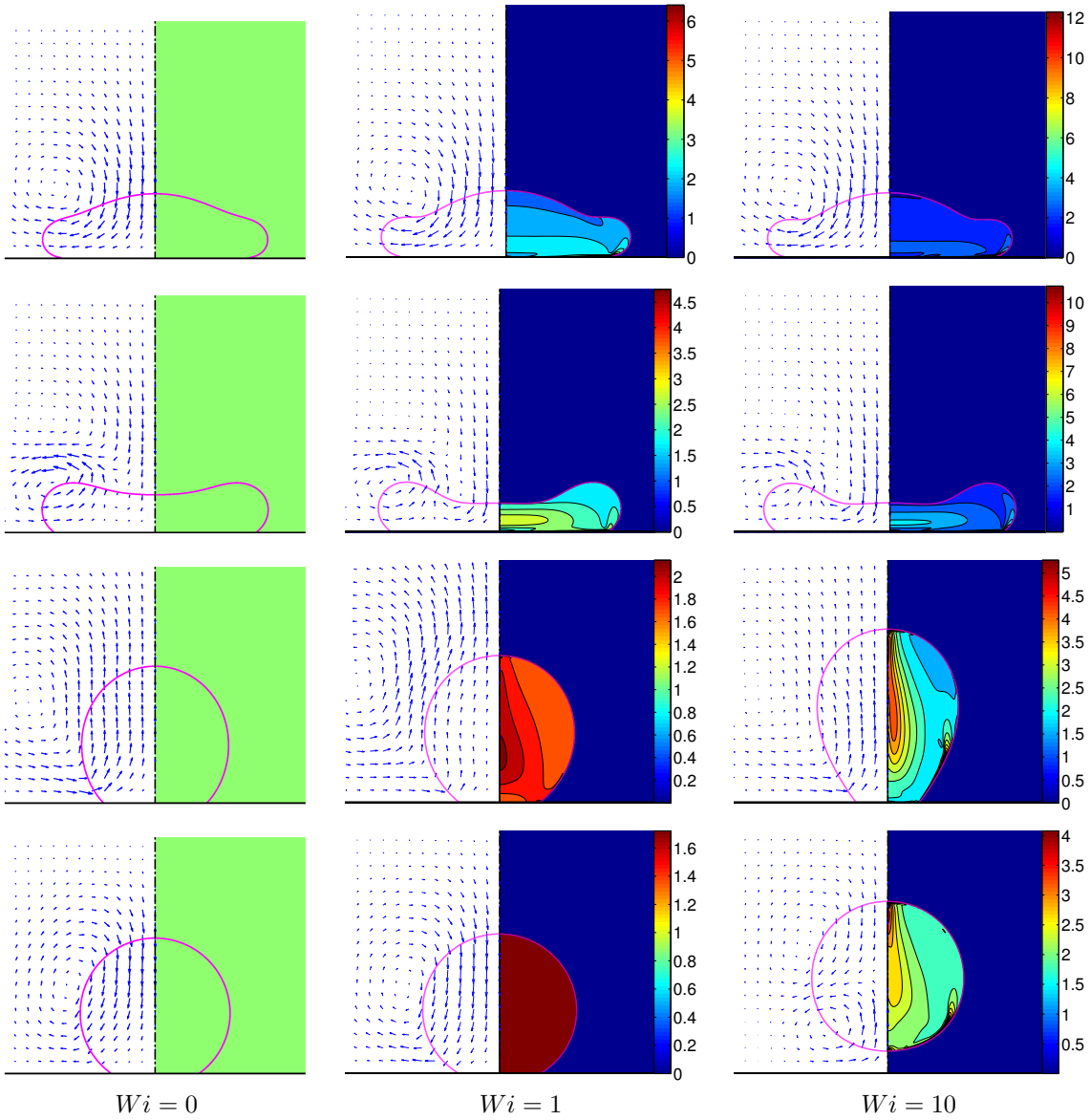

Figure 5: Effects of Wi on drop impact. The time evolution is from top to bottom. The velocity vectors are plotted on the left and the contours of average polymer extension $\sqrt{\text{trace}(\mathbf{A})}$ on the right. The snapshots are taken at the times $t^* = 0.7, 1.3, 5.0, 7.5$. ($Re = 35, We = 30, L^2 = 225$, $c = 1.27$ and $\theta_e = 145°$).

4 Conclusion and Future Work

A front-tracking method is developed for direct numerical simulations of viscoelastic interfacial flows. The log-conformation scheme is used to integrate the viscoelastic constitutive equations in time and is found to be very robust for a wide range of Weissenberg numbers. The method is first validated for single-phase viscoelastic flows including a startup flow in a circular channel. Then it is applied to buoyancy-driven motion of viscoelastic two-phase systems. The results are compared and found to be in good qualitative and quantitative agreement with the computational simulations of You et al. [14]. Finally the method is applied to study more challenging cases such as the motion of viscoelastic droplet in a pressure-driven contraction/expansion channel and viscoelastic impact and spreading on a solid surface. It is found that log-conformation method is convergent and very robust for a wide range of Weissenberg numbers.

The future work includes the application of the present method to study the effects of viscoelasticity on impact of a compound droplet on a flat surface and on a drop formation in a flow focusing configuration. Moreover, a new front-tracking method will be developed for direct numerical simulations of viscoelastic single and multiphase flows in full 3D.

References

[1] R. I. Tanner. *Engineering Rheology*. Oxford University Press, 2000.

[2] R. G. Owens and T. N. Phillips. *Computational Rheology*. Imperial College Press, 2000.

[3] G. Tryggvason, B. Bunner, A. Esmaeeli, D. Juric, N. Al-Rawahi, W. Tauber, J. Han, S. Nas, and Y.-J. Jan. A front-tracking method for the computations of multiphase flow. *J. Comput. Phys.*, 169(2):708–759, 2001.

[4] M. Muradoglu and G. Tryggvason. Simulations of soluble surfactants in 3d multiphase flow. *J. Comput. Phys.*, 274:737–757, 2014.

[5] D. Izbassarov and M. Muradoglu. A front-tracking method for computational modeling of viscoelastic two-phase flow systems. *J. Non-Newtonian Fluid Mech.*, 223:122–140, 2015.

[6] D. Izbassarov and M. Muradoglu. A computational study of two-phase viscoelastic systems in a capillary tube with a sudden contraction/expansion. *Phys. Fluids*, 28(1):012110, 2016.

[7] D. Izbassarov and M. Muradoglu. Effects of viscoelasticity on drop impact and spreading on a solid surface. *Phys. Rev. Fluids*, 1(2):023302, 2016.

[8] M.D. Chilcott and J.M. Rallison. Creeping flow of dilute polymer solutions past cylinders and spheres. *J. Non-Newtonian Fluid Mech.*, 29:381 – 432, 1988.

[9] P. J. Coates, R. C. Armstrong, and R. A. Brown. Calculation of steady-state viscoelastic flow through axisymmetric contractions with the eeme formulation. *J. Non-Newtonian Fluid Mech.*, 42(1):141 – 188, 1992.

[10] R. Borges, M. Carmona, B. Costa, and W. S. Don. An improved weighted essentially non-oscillatory scheme for hyperbolic conservation laws. *J. Comput. Phys.*, 227(6):3191 – 3211, 2008.

[11] S. O. Unverdi and G. Tryggvason. A front-tracking method for viscous, incompressible, multi-fluid flows. *J. Comput. Phys.*, 100(1):25–37, 1992.

[12] R. Fattal and R. Kupferman. Time-dependent simulation of viscoelastic flows at high weissenberg number using the log-conformation representation. *J. Non-Newtonian Fluid Mech.*, 126(1):23–37, 2005.

[13] N. D. Waters and M. J. King. The unsteady flow of an elastico-viscous liquid in a straight pipe of circular cross section. *J. Phys. D: Appl. Phys.*, 4(2):204, 1971.

[14] R. You, A. Borhan, and H. Haj-Hariri. A finite volume formulation for simulating drop motion in a viscoelastic two-phase system. *J. Non-Newtonian Fluid Mech.*, 153(2-3):109 – 129, 2008.

[15] M.F. Tome, N. Mangiavacchi, J.A. Cuminato, A. Castelo, and S. McKee. A finite difference technique for simulating unsteady viscoelastic free surface flows. *J. Non-Newtonian Fluid Mech.*, 106(2-3):61 – 106, 2002.

[16] J. Fang, R. G. Owens, L. Tacher, and A. Parriaux. A numerical study of the sph method for simulating transient viscoelastic free surface flows. *J. Non-Newtonian Fluid Mech.*, 139(1-2):68 – 84, 2006.

[17] V. Bertola. An experimental study of bouncing leidenfrost drops: Comparison between newtonian and viscoelastic liquids. *Int. J. Heat Mass Transfer*, 52(7-8):1786 – 1793, 2009.